Inorganic Chemistry

Article

pubs.acs.org/IC

Molecular Magnetic Investigation of a Family of Octanuclear [Cu_6Ln_2] Nanoclusters

Shufang Xue,[†,‡] Yun-Nan Guo,[§] Lang Zhao,[†] Haixia Zhang,[†,‡] and Jinkui Tang*[,†]

[†]State Key Laboratory of Rare Earth Resource Utilization, Changchun Institute of Applied Chemistry, Chinese Academy of Sciences, Changchun 130022, People's Republic of China

[‡]University of Chinese Academy of Sciences, Beijing 100039, People's Republic of China

[§]School of Science, Xi'an Jiaotong University, Xi'an 710049, People's Republic of China

Supporting Information

ABSTRACT: Reaction of in situ prepared acylhydrazone ligand with $Ln(NO_3)_3{\cdot}6H_2O$ and $Cu(OAc)_2{\cdot}H_2O$ resulted in the formation of novel isostructural octanuclear Cu_6Ln_2 compounds (Ln = Dy (**1**), Tb (**2**), Gd (**3**), Y (**4**)) with an unprecedented octametallic structure, which can be described as an oblate wheel built up from two structurally similar Cu_3 fragments linked together by two nodelike mononuclear lanthanide units. A detailed magnetic analysis reveals that the strong antiferromagnetic Cu···Cu interactions via the Cu−N−N−Cu−N−N−Cu linkage and the anticipated ferromagnetic Cu···Gd coupling makes an overall high-spin ground state in favor of the observation of significant magnetic caloric and SMM-like properties in the isotropic and anisotropic derivatives.

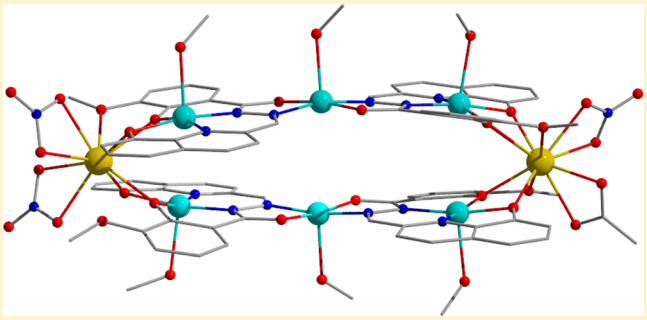

INTRODUCTION

A recurrent topic in molecular magnetism is that of the promise for spin-dependent electronics and magnetic information storage.[1] In fact, the explosive development of this topic in the last two decades have been ignited by a type of magnetic molecule displaying a blocked magnetization at low temperature and magnetic hysteresis of molecular origin.[2] These materials, generally known by the evocative name of single-molecule magnets (SMMs), are in essence molecules with a large magnetic moment and a strong magnetic anisotropy, from transition-metal-based coordination clusters to those involving anisotropic heavy lanthanide spin carriers.[3] Equally remarkable has been their outperforming application to low-temperature magnetic coolers in comparison to any conventionally employed solid-state refrigerant material, brought about by isotropic molecular nanomagnets.[4] Key ingredients to build molecular coolers rely on a large spin multiplicity associated with a negligible anisotropy.[5] To satisfy this first requisite, one efficient strategy involves the f^7 Gd^{III} ion. The inherently weak exchange mediated through the corelike f orbital of Gd^{III} and its isotropic electronic configuration guarantee the presence of multiple low-lying spin states in homo- or heterometallic (Gd^{III}−3d) clusters.[4c]

An aspect that has been worth emphasizing is that magnetic coupling has been known to be of tremendous importance in enhancing the performance of SMMs[6] or the magnetic caloric effect (MCE).[7] For SMMs, in some cases, the diffuse p orbital of the paramagnetic (usually referred to as radicals)[6b,d,8] or diamagnetic ligands[6a,c,9] can be expected to penetrate into the shielded 4f orbital to enhance exchange coupling with the lanthanide centers via a superexchange interaction. The magnetic interaction for the MCE sets the way where the magnetic entropy is released to a maximum extent in the temperature range of coupling interest.[10]

Given the prerequisite of SMMs and magnetic refrigerants, a sensible starting point is the synthesis of low-molecular-mass ferromagnetic coupling systems. In this respect, we focused on Gd^{III}−Cu^{II} clusters, as previous studies have shown this combination favors ferromagnetic exchange.[11] A rather remarkable new family of octanuclear compounds Cu_6Ln_2 (Ln = Dy (**1**), Tb (**2**), Gd (**3**), Y (**4**)) were prepared by a one-pot in situ synthesis (Scheme 1). This unprecedented octametallic topology can be described as an oblate wheel built up from two structurally similar Cu_3 fragments linked together by two nodelike mononuclear lanthanide units. The detailed magnetic properties of these compounds are reported, including the magnetic coupling between the Cu···Cu and Cu···Ln combinations, SMM properties of the anisotropic Cu_6Dy_2 and Cu_6Tb_2 analogues, and the magnetocaloric effect of an isotropic Cu_6Gd_2 derivative.

EXPERIMENTAL SECTION

General Procedures. All chemicals were used as commercially obtained without further purification. Elemental analyses for carbon, hydrogen, and nitrogen were carried out on a PerkinElmer 2400

Received: May 26, 2014
Published: July 15, 2014

dx.doi.org/10.1021/ic501226v | Inorg. Chem. 2014, 53, 8165−8171

Scheme 1. Synthesis of Compounds 1−4[a]

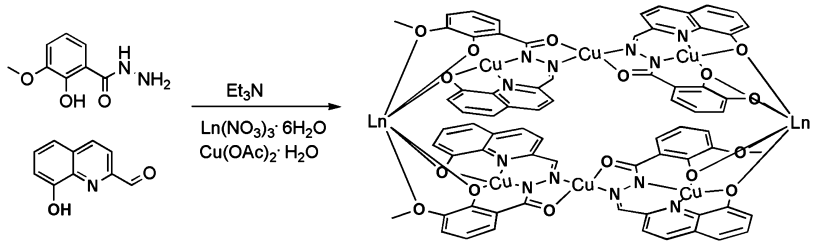

[a]Simplified drawing with the required coordination groups, counterions, and solvent molecules omitted.

Table 1. Crystallographic Data and Structure Refinement Details for 1−4

	1 (Cu_6Dy_2)	2 (Cu_6Tb_2)	3 (Cu_6Gd_2)	4 (Cu_6Y_2)
formula	$C_{85}H_{94}N_{16}O_{43}Cu_6Dy_2$	$C_{82}H_{94}N_{16}O_{46}Cu_6Tb_2$		
formula wt	2734.00	2738.81		
cryst syst	triclinic	triclinic	triclinic	triclinic
space group	$P\bar{1}$	$P\bar{1}$	$P\bar{1}$	$P\bar{1}$
T (K)	191(2)	191(2)	273(2)	273(2)
color	brown	brown	brown	brown
a (Å)	14.5113(7)	13.7210(9)	13.7450	14.5052
b (Å)	17.9030(8)	17.2254(11)	17.1614	17.8614
c (Å)	21.1473(10)	23.0876(14)	23.1423	21.1423
α (deg)	99.3110(10)	107.0910(10)	106.963	99.332
β (deg)	102.1380(10)	101.4210(10)	101.861	101.861
γ (deg)	91.5780(10)	94.6250(10)	94.536	91.536
V (Å^3)	5289.6(4)	5056.1(6)	5279.06	5279.06
Z	2	2		
D_{calcd} (g cm^{-3})	1.717	1.799		
dimens (mm)	0.26 × 0.22 × 0.14	0.24 × 0.20 × 0.18		
μ (mm^{-1})	2.670	2.717		
F(000)	2732	2740		
R_{int}	0.0329	0.0520		
no. of rflns collected	27097	25789		
no. of unique rflns	18585	17693		

analyzer. Fourier transform infrared (FTIR) spectra were recorded with a PerkinElmer FTIR spectrophotometer using the reflectance technique (4000−300 cm^{-1}). Samples were prepared as KBr disks. All magnetization data were recorded on a Quantum Design MPMS-XL7 SQUID magnetometer. The variable-temperature magnetization was measured with an external magnetic field of 1000 Oe in the temperature range of 1.9−300 K. Samples were restrained in eicosane to prevent torquing. The experimental magnetic susceptibility data are corrected for the diamagnetism estimated from Pascal's tables[12] and sample holder calibration.

X-ray Crystallography. Suitable single crystals were selected for single-crystal X-ray diffraction analysis. Crystallographic data were collected at a temperature of 191 K on a Bruker Apex II CCD diffractometer with graphite-monochromated Mo Kα radiation (λ = 0.71073 Å). Data processing was accomplished with the SAINT processing program. The structure was solved by direct methods and refined on F^2 by full-matrix least squares using SHELXTL97.[13] The location of the Dy atom was easily determined, and the O, N, and C atoms were subsequently determined from the difference Fourier maps. The non-H atoms were refined anisotropically. The H atoms were introduced in calculated positions and refined with fixed geometry with respect to their carrier atoms. Isotropic treatment has been done with the solvent molecules. CCDC 977611 (**1**) and 977612 (**2**) contain supplementary crystallographic data for this paper. These data can be obtained free of charge from the Cambridge Crystallographic Data Centre via www.ccdc.cam.ac.uk/data_request/cif.

Synthesis of $[Cu_6Dy_2(L^{3-})_4(NO_3)_3(OAc)(CH_3OH)_6]\cdot NO_3\cdot OAc\cdot 3CH_3OH\cdot 2H_2O$ (1). *o*-Vanilloylhydrazine (18.7 mg, 0.1 mmol) and 8-hydroxyquinoline-2-carbaldehyde (17.3 mg, 0.1 mmol) were dissolved in a methanol/dichloromethane (10 mL/10 mL) mixture. Then, triethylamine (0.14 mL, 0.2 mmol) was added dropwise with stirring. To the resulting solution were added $Dy(NO_3)_3\cdot 6H_2O$ (91.2 mg, 0.2 mmol) and $Cu(OAc)_2\cdot H_2O$ (39.9 mg, 0.2 mmol), and the subsequent mixture was stirred for another 5 h. The solution was then filtered and left undisturbed. Within 5 days, dark brown crystals had formed and were collected, washed with diethyl ether, and dried under vacuum. Yield: 44% based on Dy. Anal. Calcd (found) for $C_{82}H_{78}N_{16}O_{38}Cu_6Dy_2\cdot 3CH_3OH\cdot 2H_2O$: C, 37.34 (36.94); H, 3.47 (3.42); N, 8.20 (8.04). IR (KBr, cm^{-1}): 3363 (br), 3054 (br), 1592 (w), 1552 (w), 1495 (s), 1463 (s), 1387 (s), 1367 (s), 1343 (s), 1321 (s), 1224 (m), 1197 (m), 1090 (w), 1047 (w), 976 (w), 838 (w), 792 (w), 747 (w), 688 (w), 625 (w), 493 (w).

Synthesis of $[Cu_6Tb_2(L^{3-})_4(NO_3)_3(OAc)_2(CH_3OH)_5]\cdot NO_3\cdot CH_3OH\cdot 6H_2O$ (2). This compound was prepared as for **1**, but $Tb(NO_3)_3\cdot 6H_2O$ (90.6 mg, 0.2 mmol) was used in place of $Dy(NO_3)_3\cdot 6H_2O$. Yield: 51% based on Tb. Anal. Calcd (found) for $C_{81}H_{78}N_{16}O_{39}Cu_6Tb_2\cdot CH_3OH\cdot 6H_2O$: C, 35.96 (35.58); H, 3.46 (3.35); N, 8.18 (8.10). IR (KBr, cm^{-1}): 3361 (br), 3060 (br), 1604 (w), 1592 (w), 1495 (s), 1462 (s), 1386 (s), 1366 (s), 1344 (s), 1321 (s), 1232 (m), 1198 (m), 1163 (w), 1115 (w), 1090 (w), 1049 (w), 976 (w), 838 (w), 792 (w), 747 (w), 687 (w), 625 (w), 492 (w).

Synthesis of $[Cu_6Gd_2]$ (3). This compound was prepared as for **1**, but $Gd(NO_3)_3\cdot 6H_2O$ (90.2 mg, 0.2 mmol) was used in place of $Dy(NO_3)_3\cdot 6H_2O$. Yield: 37% based on Gd. Anal. Calcd for $C_{81}H_{78}N_{16}O_{39}Cu_6Gd_2$ (dried): C, 37.49; H, 3.03; N, 8.63. Found for **3**: C, 37.05; H, 2.92; N, 8.68. IR (KBr, cm^{-1}): 3375 (br), 3060 (br), 1592 (w), 1495 (s), 1462 (s), 1386 (s), 1365 (s), 1344 (s), 1321 (s),

dx.doi.org/10.1021/ic501226v | Inorg. Chem. 2014, 53, 8165−8171

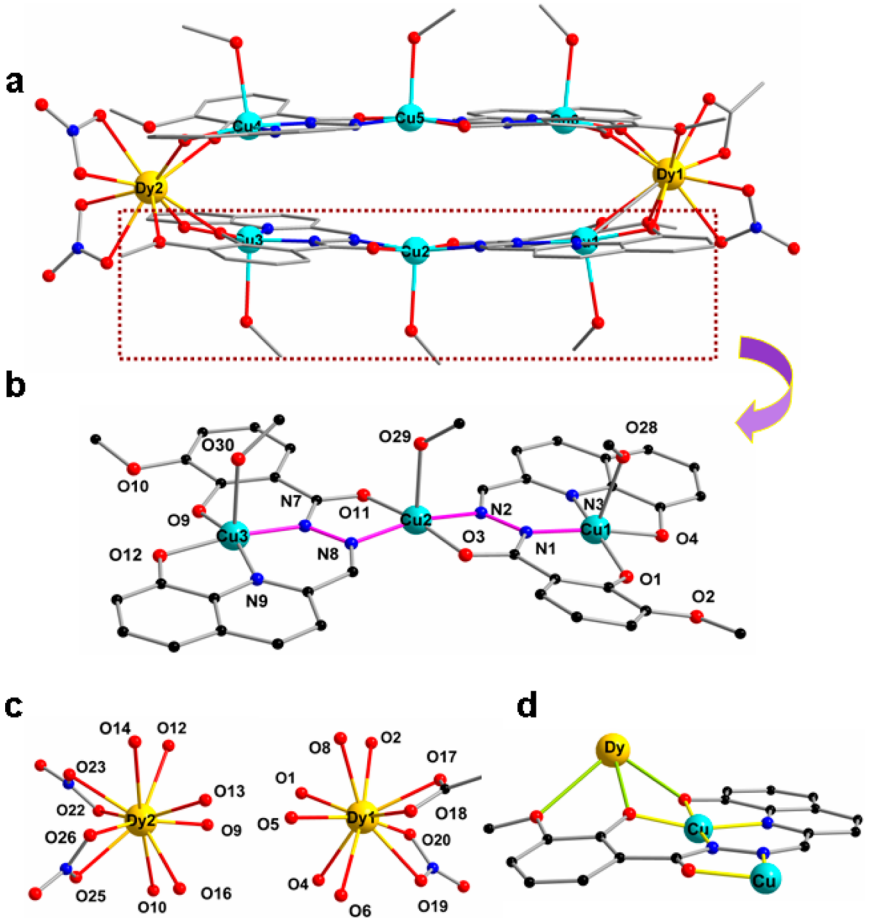

Figure 1. Representation of the structure of the Cu_6Dy_2 cationic entity (a), the nearly linear Cu_3 subunit (b), the coordination spheres of the Dy^{III} centers (c), and the coordination mode of the ligand (d) in **1**.

1232 (m), 1197 (m), 1162 (w), 1115 (w), 1089 (w), 1048 (w), 976 (w), 838 (w), 792 (w), 747 (w), 687 (w), 625 (w), 493 (w).

Synthesis of $[Cu_6Y_2]$ (4). This compound was prepared as for **1**, but $Y(NO_3)_3{\cdot}6H_2O$ (76.6 mg, 0.2 mmol) was used in place of $Dy(NO_3)_3{\cdot}6H_2O$. Yield: 40% based on Y. Anal. Calcd for $C_{82}H_{78}N_{16}O_{38}Cu_6Y_2$ (dried): C, 40.12; H, 3.20; N, 9.13. Found for **3**: C, 39.70; H, 3.05; N, 9.06. IR (KBr, cm^{-1}): 3374 (br), 3048 (br), 1592 (w), 1556 (w), 1494 (s), 1463 (s), 1387 (m), 1368 (m), 1342 (m), 1321 (s), 1223 (w), 1196 (w), 1088 (w), 1044 (w), 976 (w), 837 (w), 791 (w), 747 (w), 688 (w), 625 (w), 492 (w).

RESULTS AND DISCUSSION

Compounds **1**–**4** were isolated from the reaction of $Cu(OAc)_2{\cdot}H_2O$, $Ln(NO_3)_3{\cdot}6H_2O$, proligand H_3L, and triethylamine in the mixture of methanol and dichloromethane after 5 days (Scheme 1). Full structure determinations were carried out for **1** and **2**, and the remaining two compounds were shown to be isomorphous from their unit cells (Table 1), powder X-ray diffraction patterns (Figure S1, Supporting Information) and IR spectra (Figure S2, Supporting Information). Single-crystal analysis reveals that compounds **1** and **2** are structurally analogous, differing only in the coordinated terminal ions and the number of cocrystallized solvent molecules, as observed in the molecular formulas $[Dy_2Cu_6(L^{3-})_4(NO_3)_3(OAc)(CH_3OH)_6]{\cdot}NO_3{\cdot}OAc{\cdot}3CH_3OH{\cdot}2H_2O$ (**1**) and $[Tb_2Cu_6(L^{3-})_4(NO_3)_3(OAc)_2(CH_3OH)_5]{\cdot}NO_3{\cdot}CH_3OH{\cdot}6H_2O$ (**2**), and so for the sake of brevity we will limit our discussion to compound **1**, highlighting any specific differences between the molecules at the appropriate stages.

Compound **1** crystallizes in the triclinic space group $P\bar{1}$ with $Z = 2$ and consists of the complex cation $[Dy_2Cu_6(L)_4(NO_3)_3(OAc)(CH_3OH)_6]^{2+}$ crystallizing with nitrate and acetate anions for charge balance. The octametallic cationic entity (Figure 1a), connected by four fully deprotonated compartment ligands, can be described as an oblate wheel built up from two structurally similar Cu_3 fragments (Figure 1b) linked together by two nodelike mononuclear [Dy] units (Figure 1c). Each ligand L^{3-} coordinates to three metallic centers in a μ_3-η^1:η^2:η^1:η^1:η^1:η^1:η^2 coordination mode by programmed target sites—in accord with to hard Lewis bases (HSAB theory),[14] the bidentate *o*-vanillin group is preferable to the harder dysprosium(III) ion while the central quadridentate ONNO pocket prefers the softer copper(II) ion (Figure 1d).

Each Cu_3 fragment is assembled by two triply deprotonated polydentate ligands bridging three copper(II) ions in the same quadridentate (ONNO)–bidentate ($O_{carbonyl}N_{imine}$) binding mode, leading to a linear trinuclear unit with four Cu–N–N–Cu torsion angles of −172.4, −177.5, −173.3, and −177.4°. Such an N–N bridge is very important mode for hydrazone ligands to construct linear[15] or macrocyclic[16] compounds. Two terminal Cu^{II} ions, Cu1 and Cu3, are in a five-coordinated CuN_2O_3 square-pyramidal geometry with phenolic oxygen atoms (O1 and O4 for Cu1, O9 and O12 for Cu3), which also chelate the harder Dy^{III} ion, hydrazine nitrogen (N1 for Cu1 and N7 for Cu3), and pyridine nitrogen (N3 for Cu1 and N9 for Cu3) atoms in the *cis* formal equatorial plane. Cu2, however, in the center, also adopts a square-pyramidal

dx.doi.org/10.1021/ic501226v | *Inorg. Chem.* 2014, 53, 8165–8171

geometry with two carbonyl oxygen atoms (O3 and O11) and two imine nitrogen atoms (N2 and N8) from two ligands as is characteristic of a *trans* formal basal plane (Figure 2). The axial

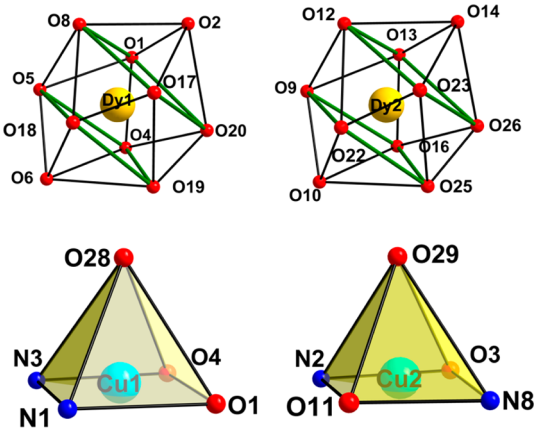

Figure 2. Coordination polyhedra observed in **1**: a distorted-bicapped-square-antiprismatic geometry for Dy and a square-pyramidal environment for Cu.

positions are occupied by methanol molecules with a longer Cu−O distance in the range of 2.2382(7)−2.3329(6) Å, which causes the coordination sphere of the five-coordinated Cu^{II} to slightly deviate from the ideal pyramidal geometry (Table S2, Supporting Information). The average separation of adjacent copper(II) ions is equal to 4.7033 Å, but a relatively shorter separation with a distance of 3.7371(15)−3.9398(15) Å is observable between Cu_3 fragments.

Two nodelike dysprosium(III) ions are coordinated to the bidentate *o*-vanillin group and the phenol oxygen atoms derived from ligands as well as the counterions (nitrate or acetate) in a η^2 fashion, affording a O_{10} coordination sphere in a bicapped-square-antiprismatic geometry determined by using SHAPE 2.0 software[17] (Figure 2 and Table S2 (Supporting Information)).

Within the eight phenoxide Cu···Dy linkages, Cu−O and Dy−O bond lengths are in the ranges 1.878(6)−1.986(6) and 2.323(6)−2.461(5) Å and the Cu−O−Dy angles in the range 98.4(2)−105.9(2)°. The Dy···Cu separations range from 3.3470(12) to 3.3792(11) Å.

The structure of the cationic entity in **2** is essentially isomorphous with **1**, as shown in Figure 3, the only difference being the ligand bridging between the axial sites on Cu5 and Tb2. Another terminal monodentate nitrate ion is weakly bonded to Cu5 in the apical position in **2** rather than the solvent methanol group in **1**. One acetate ion and one nitrate ion occupy the required coordination pockets of two nodelike Tb^{III} ions, making them 10-coordinate.

Magnetic Properties. Variable-temperature direct-current (dc) magnetic susceptibilities of **1**−**4** were carried out on powder samples embedded in eicosane in the temperature range 2.0−300 K with a 1000 Oe applied magnetic field. The dc magnetic data were displayed and summarized in Figure 4 and Table 2.

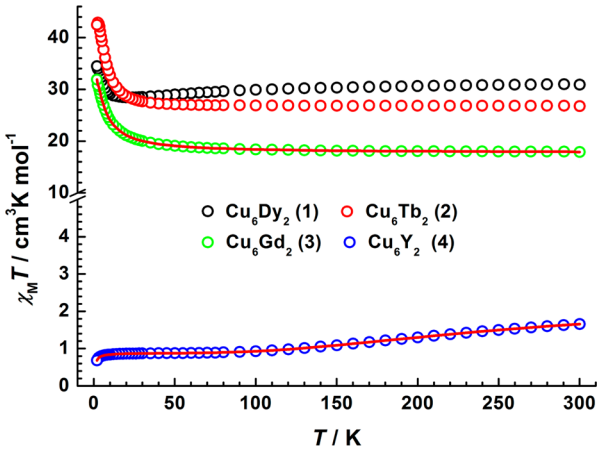

Figure 4. Temperature dependence of the $\chi_M T$ product (with χ defined as molar magnetic susceptibility equal to M/H per mole) at 1000 Oe for compounds **1**−**4**. The red lines correspond to the calculated behavior of compounds **3** and **4** (see the text for details).

Direct current (dc) magnetic susceptibility measurements show the room-temperature $\chi_M T$ products estimated as 30.89 (**1**), 26.76 (**2**) and 17.88 cm^3 K mol^{-1} (**3**) are in relatively good agreement with the presence of six Cu^{II} ions ($S = {}^1/_2$, $g = 2$, $C =$ 0.375 cm^3 K mol^{-1}) and two lanthanide metal ions: two Dy^{III} metal ions ($S = {}^5/_2$, $L = 5$, $^6H_{15/2}$, $g = {}^4/_3$) for **1**, two Tb^{III} metal ions ($S = 3$, $L = 3$, $^7F_6$, $g = {}^5/_4$) for **2**, and two Gd^{III} metal ions ($S = {}^7/_2$, $L = 0$, $^8S_{7/2}$, $g = 2$) for **3**. For **4**, however, the observed

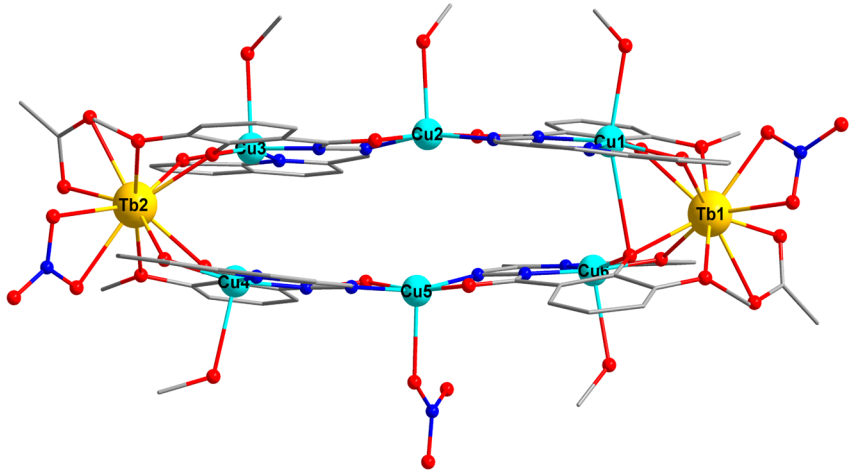

Figure 3. Representation of the structure of the Cu_6Tb_2 cationic entity in **2**.

dx.doi.org/10.1021/ic501226v | *Inorg. Chem.* 2014, 53, 8165−8171

Table 2. Magnetic Data Extracted from the Static Properties of 1−4

	1	2	3	4
ground state term of Ln^{III} ion	$^6H_{15/2}$	$^7F_6$	$^8S_{7/2}$	
C (cm^3 K mol^{-1}) for each Ln^{III} ion	14.17	11.82	7.875	0
χT (cm^3 K mol^{-1}) expected/exptl value at room temp	30.59/30.89	25.89/26.76	18/17.88	2.25/1.66
χT (cm^3 K mol^{-1}) exptl value at 2.0 K	34.44	42.45	31.88	0.68
magnetization (μ_B) obsd at 7 T and 2.0 K	14.07	14.10	16.80	2.07

$\chi_M T$ value equal to 1.66 cm^3 K mol^{-1} at 300 K is apparently far from the expected value of 2.25 cm^3 K mol^{-1} for six uncoupled/independent Cu^{II} ions (g = 2.0) due to noncontributing diamagnetic Y^{III} ions (Figure 4), indicating that a strong antiferromagnetic interaction predominates between Cu^{II} ions.[18]

As shown in Figure 4, thermal evolutions for **1**−**3** are very similar. The $\chi_M T$ product abruptly increases to reach the corresponding maxima of 34.44, 42.44, and 31.88 cm^3 K mol^{-1} at 2 K after a feeble decrease below 100 K, indicating the presence of ferromagnetic interactions with high-spin ground states, which is emphasized by the temperature dependence of the difference in $\chi_M T$ values between **3** and **4**, $\Delta\chi_M T$ = $(\chi_M T)(Cu_6Gd_2)$ − $(\chi_M T)(Cu_6Y_2)$ (Figure S3, Supporting Information). The increase in $\Delta\chi_M T$ versus T can be ascribed to Gd···Cu ferromagnetic interactions through a bridging GdO_2Cu linker. In order to quantify those magnetic couplings, we simulated the magnetic properties by using the two coupling parameters J_1 (Cu1Cu2, Cu2Cu3, Cu4Cu5, and Cu5Cu6) and J_2 (Cu1Gd2, Cu6Gd2, Cu3Gd1 and Cu4Gd1), taking into consideration the couplings propagated by bridges, as shown in Figure 5. Fitting the experimental data for **3** and **4** with the

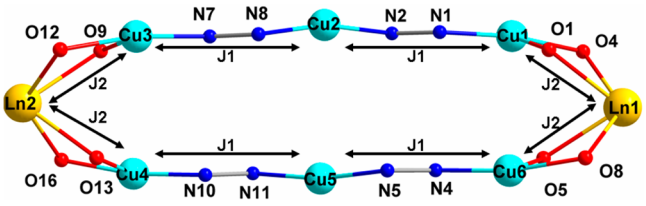

Figure 5. Schematic diagram for the Cu_6Ln_2 core and potential magnetic coupling pathways.

MAGPACK program package[19] provides a set of parameters: J_1 = −110.0 cm^{-1}, J_2 = 0.96 cm^{-1}, and g = 2.10 for **3** and J_1 = −107.5 cm^{-1} and g = 2.12 for **4**. The simulated results indicate that Cu^{II} ions strongly interact through a superexchange mechanism operating via Cu−N−N−Cu−N−N−Cu linkages,[20] thus leading to an S_T = $^1/_2$ spin ground state for **4** with an $E(^1/_2,0)$ first excited state lying +107.5 cm^{-1} above the ground state,[12] which can be confirmed from the field dependence of magnetization at 1.9 K (Figure 6). On the basis of **4**, the ferromagnetic contribution is unquestionably derived from the Gd−O_2−Cu coupling, as has been noted for a number of Gd^{III} and Cu^{II} ions bridged by two oxygen atoms.[4c,21] Additionally, the ground state in **3** is found to be S = 8, as evidenced from the isothermal magnetization data, for which the magnetization saturates at fields larger than 1 T and

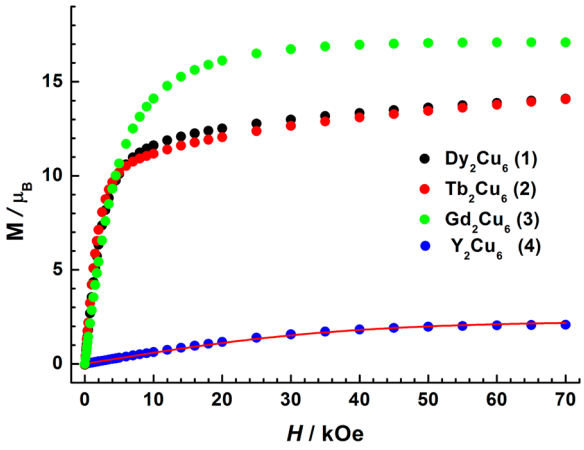

Figure 6. Field dependences of magnetization at 1.9 K in the field range 0−70 kOe. The solid line gives the fit made with the same parameters as for $\chi_M T$ for **4**.

reaches 16.0 μ_B at 7 T (Figure 6). The isothermal magnetization data for **1** and **2** at different temperatures are not superposed on a master curve and do not approach the saturation (Figure S4, Supporting Information), suggesting the presence of magnetic anisotropy and/or low-lying excited states, as expected for a compound containing anisotropic Dy^{III} or Tb^{III} ions.

In order to explore the dynamics of **1** and **2**, alternating current (ac) susceptibility measurements were performed in a 3 Oe ac field with a 0 applied dc field, which show temperature-dependent (Figure 7, for **1**) or frequency-dependent (Figure 8,

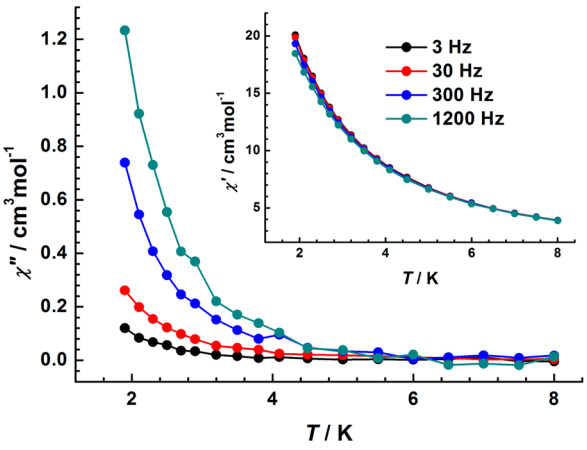

Figure 7. Temperature-dependent ac susceptibility data for **1** collected under 0 dc field at the indicated frequency.

for **2**) out-of phase (χ'') signals, indicating the onset of slow magnetization relaxation. Due to the lack of the peaks in $\chi''(T)$ plots, for **1**, we have employed another method[22] to estimate the energy barrier and relaxation time with the parameters U_{eff} ≈ 5.2 K and τ_0 ≈ 6.5 × 10^{-6} s (Figure S5, Supporting Information). For **2**, the in-phase component shows strong frequency dependence, and below 4 K, the out-of-phase component becomes nonzero and frequency-dependent maxima are observable at the indicated temperatures (Figure 8), as expected for an SMM. The relaxation time (τ) extracted from the frequency-dependent $\chi''(\upsilon)$ versus T^{-1} plot (Figure 8) fits well to a simple Arrhenius law with U_{eff} = 15.6(1) K and τ_0 = [6.9(2)] × 10^{-7} s. This result indicates that the relaxation of

dx.doi.org/10.1021/ic501226v | Inorg. Chem. 2014, 53, 8165−8171

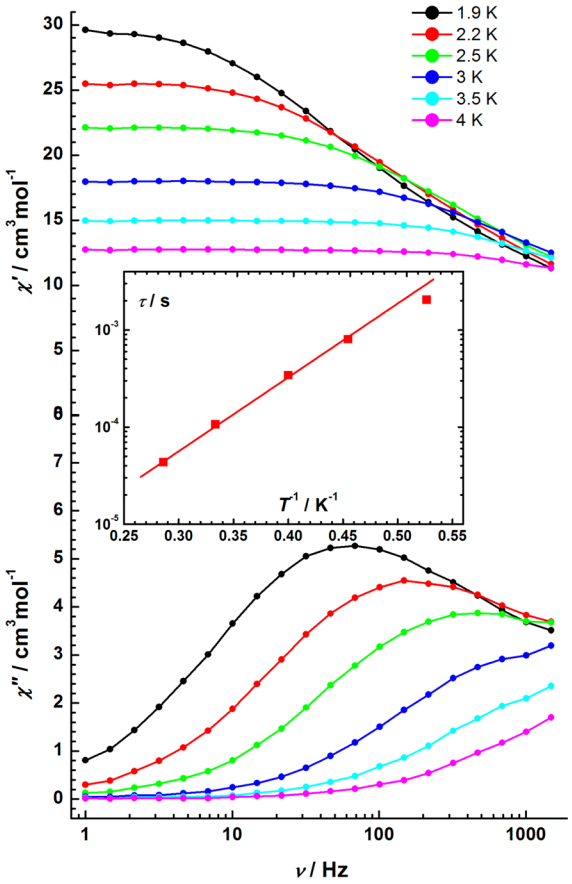

Figure 8. Frequency dependence of the in-phase (top) and out-of phase (bottom) components of ac susceptibility for **2** at the indicated temperatures under 0 dc field. Inset: relaxation time (τ) versus T^{-1} plot (red squares) and the Arrhenius fit (red line).

the magnetization is governed by a thermally activated process above 1.9 K.[23]

On account of the large magnetization value and the relatively large magnetic density, we explored the magnetic entropy changes ΔS_m as a key parameter in evaluating MCE on **3**. The ΔS_m value can be calculated on the basis of the experimental magnetization data (Figure 9) and the Maxwell equation $\Delta S_m(T)_{\Delta H} = \int[\partial M(T,H)/\partial T]_H \, dH$.[5] The resulting ΔS_m values at different magnetic fields and temperatures are exemplified in Figure 10, where the maximum entropy change

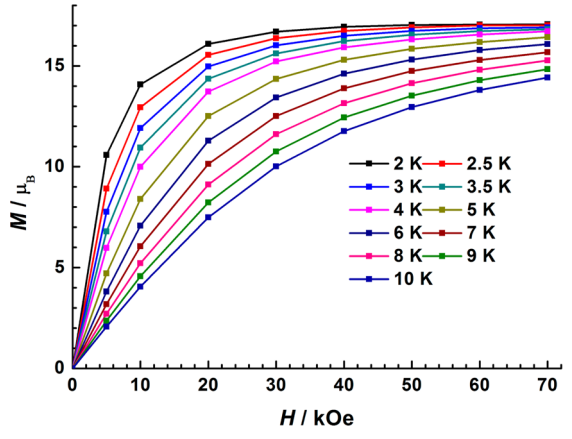

Figure 9. Field-dependent magnetization plots for **3** from 2 to 10 K.

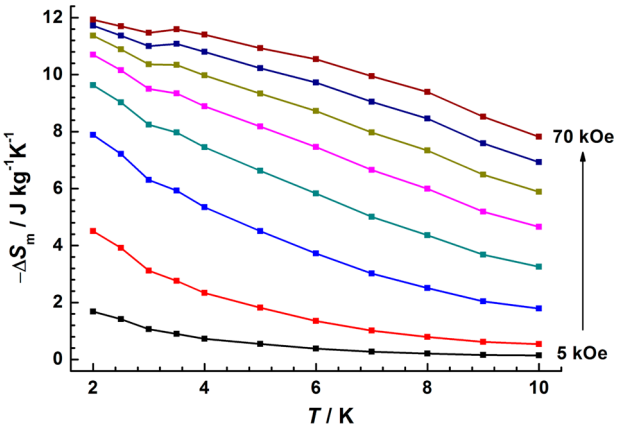

Figure 10. Magnetic entropy changes (ΔS_m) calculated using the magnetization data for **3** at fields from 5 to 70 kOe and temperatures from 2 to 10 K.

of 11.9 J kg^{-1} K^{-1} is obtained at 2 K for ΔH = 70 kOe corresponding to $2S_{Gd}$ and $2S_T$ (Cu_3, $^1/_2$) calculated as 16.6 J kg^{-1} K^{-1}. However, it is smaller than the theoretical value of 25.28 J kg^{-1} K^{-1} calculated for two Gd^{III} ($S = {}^7/_2$) and six Cu^{II} ($S = {}^1/_2$) fully decoupled ions using the equation $-\Delta S_m = nR \ln(2S + 1) = 2R \ln 8 + 6R \ln 2$. This may be due to the main "con" that the strong antiferromagnetic coupling between Cu^{II} ions within Cu_3 subunits contributes passively to the observation of maximum MCE with reference to Cu_5Gd_4[4c] and Cu_6Gd_6,[21] where the weaker coupling promotes a relatively larger number of low-lying excited spin states, thus leading to a larger field dependence of the MCE.[24]

CONCLUSION

We report a rather remarkable new family of octanuclear Cu_6Ln_2 compounds, in which the cationic entity can be divided into two parts: two linear Cu_3 subunits and two nodelike lanthanide ions. The strong antiferromagnetic interactions arising from a superexchange mechanism via the Cu−N−N−Cu−N−N−Cu linkage and the ferromagnetic Cu···Gd coupling lead to a high spin of 8, which is responsible for the significant magnetic caloric properties of Cu_6Gd_2, and the anisotropic analogues Cu_6Dy_2 and Cu_6Tb_2 display SMM-like behavior. This work represents an efficient model to understand magnetic exchange interactions, relaxation dynamics, and magnetic caloric effects.

ASSOCIATED CONTENT

Supporting Information

Selected bond and angle data (Table S1), geometry analysis (Table S2), XRD pattern (Figure S1), IR spectra (Figure S2), magnetic measurements (Figures S3−S5), and crystallographic data for **1** and **2** (CIF files). This material is available free of charge via the Internet at http://pubs.acs.org.

AUTHOR INFORMATION

Corresponding Author

*E-mail for J.T.: tang@ciac.ac.cn.

Notes

The authors declare no competing financial interest.

dx.doi.org/10.1021/ic501226v | Inorg. Chem. 2014, 53, 8165−8171

■ ACKNOWLEDGMENTS

We thank the National Natural Science Foundation of China (Grants 21371166, 21331003 and 21221061) for financial support.

■ REFERENCES

(1) Bill, E. *Nat. Chem.* **2013**, *5*, 556−557.
(2) Gatteschi, D.; Fittipaldi, M.; Sangregorio, C.; Sorace, L. *Angew. Chem., Int. Ed.* **2012**, *51*, 4792−4800.
(3) (a) Gatteschi, D.; Sessoli, R.; Villain, J. *Molecular Nanomagnets*; Oxford University Press: Oxford, U.K., 2006. (b) Luzon, J.; Sessoli, R. *Dalton Trans.* **2012**, *41*, 13556−13567. (c) Aromí, G.; Brechin, E. K. *Struct. Bonding (Berlin)* **2006**, *122*, 1−67. (d) Woodruff, D. N.; Winpenny, R. E. P.; Layfield, R. A. *Chem. Rev.* **2013**, *113*, 5110−5148. (e) Zhang, P.; Guo, Y.-N.; Tang, J. *Coord. Chem. Rev.* **2013**, *257*, 1728−1763.
(4) (a) Evangelisti, M.; Roubeau, O.; Palacios, E.; Camón, A.; Hooper, T. N.; Brechin, E. K.; Alonso, J. J. *Angew. Chem., Int. Ed.* **2011**, *50*, 6606−6609. (b) Zheng, Y.-Z.; Evangelisti, M.; Winpenny, R. E. P. *Angew. Chem., Int. Ed.* **2011**, *50*, 3692−3695. (c) Langley, S. K.; Chilton, N. F.; Moubaraki, B.; Hooper, T.; Brechin, E. K.; Evangelisti, M.; Murray, K. S. *Chem. Sci.* **2011**, *2*, 1166−1169. (d) Sessoli, R. *Angew. Chem., Int. Ed.* **2012**, *51*, 43−45. (e) Zheng, Y.-Z.; Zhou, G.-J.; Zheng, Z.; Winpenny, R. E. P. *Chem. Soc. Rev.* **2014**, *43*, 1462−1475.
(5) Evangelisti, M.; Brechin, E. K. *Dalton Trans.* **2010**, *39*, 4672−4676.
(6) (a) Long, J.; Habib, F.; Lin, P.-H.; Korobkov, I.; Enright, G.; Ungur, L.; Wernsdorfer, W.; Chibotaru, L. F.; Murugesu, M. *J. Am. Chem. Soc.* **2011**, *133*, 5319−5328. (b) Rinehart, J. D.; Fang, M.; Evans, W. J.; Long, J. R. *Nat. Chem.* **2011**, *3*, 538−542. (c) Guo, Y.-N.; Xu, G.-F.; Wernsdorfer, W.; Ungur, L.; Guo, Y.; Tang, J.; Zhang, H.-J.; Chibotaru, L. F.; Powell, A. K. *J. Am. Chem. Soc.* **2011**, *133*, 11948−11951. (d) Demir, S.; Zadrozny, J. M.; Nippe, M.; Long, J. R. *J. Am. Chem. Soc.* **2012**, *134*, 18546−18549.
(7) (a) Hooper, T. N.; Schnack, J.; Piligkos, S.; Evangelisti, M.; Brechin, E. K. *Angew. Chem., Int. Ed.* **2012**, *51*, 4633−4636. (b) Zheng, Y.-Z.; Evangelisti, M.; Tuna, F.; Winpenny, R. E. P. *J. Am. Chem. Soc.* **2012**, *134*, 1057−1065.
(8) (a) Fatila, E. M.; Rouzières, M.; Jennings, M. C.; Lough, A. J.; Clérac, R.; Preuss, K. E. *J. Am. Chem. Soc.* **2013**, *135*, 9596−9599. (b) Bernot, K.; Bogani, L.; Caneschi, A.; Gatteschi, D.; Sessoli, R. *J. Am. Chem. Soc.* **2006**, *128*, 7947−7956.
(9) Langley, S. K.; Wielechowski, D. P.; Vieru, V.; Chilton, N. F.; Moubaraki, B.; Abrahams, B. F.; Chibotaru, L. F.; Murray, K. S. *Angew. Chem., Int. Ed.* **2013**, *52*, 12014−12019.
(10) Martínez-Pérez, M.-J.; Montero, O.; Evangelisti, M.; Luis, F.; Sesé, J.; Cardona-Serra, S.; Coronado, E. *Adv. Mater.* **2012**, *24*, 4301−4305.
(11) (a) Bencini, A.; Benelli, C.; Caneschi, A.; Carlin, R. L.; Dei, A.; Gatteschi, D. *J. Am. Chem. Soc.* **1985**, *107*, 8128−8136. (b) Wu, G.; Hewitt, I. J.; Mameri, S.; Lan, Y.; Clérac, R.; Anson, C. E.; Qiu, S.; Powell, A. K. *Inorg. Chem.* **2007**, *46*, 7229−7231.
(12) Kahn, O. *Molecular Magnetism*; Wiley-VCH: New York, 1993.
(13) Sheldrick, G. M. *SHELXS-97, Program for Crystal Structure Solution*; University of Göttingen, Göttingen, Germany, 1997.
(14) (a) Pearson, R. G. *J. Am. Chem. Soc.* **1963**, *85*, 3533−3539. (b) Pearson, R. G. *J. Chem. Educ.* **1968**, *45*, 581.
(15) (a) Zhao, L.; Thompson, L. K.; Xu, Z.; Miller, D. O.; Stirling, D. R. *J. Chem. Soc., Dalton Trans.* **2001**, 1706−1710. (b) Tandon, S. S.; Dawe, L. N.; Milway, V. A.; Collins, J. L.; Thompson, L. K. *Dalton Trans.* **2007**, 1948−1953. (c) Shi, X.; Li, D.; Wang, S.; Zeng, S.; Wang, D.; Dou, J. *J. Solid State Chem.* **2010**, *183*, 2144−2153.
(16) (a) Shuvaev, K. V.; Abedin, T. S. M.; McClary, C. A.; Dawe, L. N.; Collins, J. L.; Thompson, L. K. *Dalton Trans.* **2009**, 2926−2939. (b) Li, C.-P.; Zhao, X.-H.; Chen, X.-D.; Yu, Q.; Du, M. *Cryst. Growth Des.* **2010**, *10*, 5034−5042.
(17) Ruiz-Martínez, A.; Alvarez, S. *Chem. Eur. J.* **2009**, *15*, 7470−7480.
(18) (a) Zhang, H.; Zhuang, G.-L.; Kong, X.-J.; Ren, Y.-P.; Long, L.-S.; Huang, R.-B.; Zheng, L.-S. *Cryst. Growth Des.* **2013**, *13*, 2493−2498. (b) Chandrasekhar, V.; Dey, A.; Das, S.; Rouzières, M.; Clérac, R. *Inorg. Chem.* **2013**, *52*, 2588−2598.
(19) Borras-Almenar, J. J.; Clemente-Juan, J. M.; Coronado, E.; Tsukerblat, B. S. *Inorg. Chem.* **1999**, *38*, 6081−6088.
(20) Chen, X.; Zhan, S.; Hu, C.; Meng, Q.; Liu, Y. *J. Chem. Soc., Dalton Trans.* **1997**, 245−250.
(21) Dinca, A. S.; Ghirri, A.; Madalan, A. M.; Affronte, M.; Andruh, M. *Inorg. Chem.* **2012**, *51*, 3935−3937.
(22) Luis, F.; Bartolomé, J.; Fernández, J. F.; Tejada, J.; Hernádez, J. M.; Zhang, X. X.; Ziolo, R. *Phys. Rev. B* **1997**, *55*, 11448.
(23) Feltham, H. L. C.; Clérac, R.; Ungur, L.; Chibotaru, L. F.; Powell, A. K.; Brooker, S. *Inorg. Chem.* **2013**, *52*, 3232−3240.
(24) Chen, Y.-C.; Guo, F.-S.; Liu, J.-L.; Leng, J.-D.; Vrábel, P.; Orendáč, M.; Prokleška, J.; Sechovský, V.; Tong, M.-L. *Chem. Eur. J.* **2014**, *20*, 3029−3035.